Nanoscale Advances

ROYAL SOCIETY
OF CHEMISTRY

COMMUNICATION
Bongju Kim, Dong-Wook Han *et al.*
3D printed membranes of polylactic acid and graphene
oxide for guided bone regeneration

NCNST

COMMUNICATION

Check for updates

3D printed membranes of polylactic acid and graphene oxide for guided bone regeneration

Hee Jeong Jang,†[a] Moon Sung Kang,†[a] Won-Hyeon Kim,†[b] Hyo Jung Jo,[a] Sung-Ho Lee, [bc] Eun Jeong Hahm,[de] Jung Hyun Oh,[de] Suck Won Hong, [a] Bongju Kim *[b] and Dong-Wook Han *[af]

We fabricated graphene oxide (GO)-incorporated polylactic acid (PLA) (GO-PLA) films by using three-dimensional (3D) printing to explore their potential benefits as barrier membranes for guided bone regeneration (GBR). Our results showed that the 3D printed GO-PLA films provided highly favorable matrices for preosteoblasts and accelerated new bone formation in rat calvarial bone defect models.

Introduction

Human bones spontaneously regenerate over a lifetime, but critical damage beyond a recoverable range frequently occurs by internal or external factors such as traumatic injuries, cancers, bacterial or viral infection, and degenerative diseases.[1,2] To recover the impaired bone tissues, conventional bone grafts have been employed as structural supports or space-filling prostheses without supporting proper interactions between existing tissues and grafts.[3,4] To overcome the low biofunctionality of contemporary orthopedic implants, tissue-engineered scaffolds have been highlighted as promising bone graft alternatives with plenty of biofunctionalities to improve the recovery process, which is called osseointegration.[5,6] Acceleration of the healing process after surgery is the most priority in orthopedic implants, especially, the facilitation of fast accommodation with the surrounding environment and prolonged osseointegration of implanted grafts should be preferentially considered. Recently developed tissue-engineered bone scaffolds aim to recapitulate the structural and functional characteristics of natural bone extracellular matrix (ECM), which endow laden cells with compatible microenvironments to promote robust behaviours and appropriate phenotypes.[7–9]

Three-dimensional (3D) printing refers to the additive manufacturing of 3D constructs in the desired shape by sequentially building up bioink materials in a layer-by-layer manner. 3D printing has provided numerous benefits in the field of bone tissue engineering, such as the ability to create patient-specific grafts that precisely match the desired shape and size, serving as excellent templates for bone growth.[10] Additionally, this technology allows for precise control over the material composition enabling customization of the additive ratios. This is particularly advantageous for nanomaterials, as their toxicity and efficacy often depend on the dosage.[11,12]

Graphene, one of the novel two-dimensional (2D) nanomaterial families, is composed of two-dimensional monolayered sp^2-bonded carbon atoms and features exceptional physicochemical, electrical, and mechanical properties.[13–16] Owing to the oxygen-containing functional moieties, the incorporation of graphene oxide (GO) into PLA can enhance surface hydrophilicity and cell–matrix interaction to facilitate adhesion, proliferation, and differentiation. Despite the excellent osteogenic effects of growth factors including bone morphogenic factors (BMPs), epidermal growth factors (EGFs), and basic fibroblast growth factors (bFGFs), high costs and potential adverse effects such as ectopic bone formation, post-operative inflammation, and tumorigenesis, should be carefully considered for clinical translation.[17] Therefore, we adopted GO as an alternative strategy for osseointegration-functionalized orthopedic implants.

Meanwhile, polylactic acid (PLA) is one of the most utilized scaffold materials due to its excellent biocompatibility, biodegradability, and chemical modifiability.[18] During the synthesis of PLA from lactide, the combination of L-lactic acid and D-lactic acid, which refer to asymmetric carbon atoms, can yield different stereochemical forms. Herein, we employed a 50 : 50

[a]Department of Cogno-Mechatronics Engineering, Pusan National University, Busan 46241, Republic of Korea. E-mail: nanohan@pusan.ac.kr

[b]Dental Life Science Research Institute/Innovation Research & Support Center for Dental Science, Seoul National University Dental Hospital, Seoul 03080, Republic of Korea. E-mail: bjkim016@gmail.com

[c]Department of Oral and Maxillofacial Surgery, School of Dentistry, Seoul National University, Seoul 03080, Republic of Korea

[d]Luvantix ADM Co., Ltd, Daejeon 34050, Republic of Korea

[e]3DMaterials Co., Ltd, Anyang-si, Gyeonggi-do 14059, Republic of Korea

[f]BIO-IT Fusion Technology Research Institute, Pusan National University, Busan 46241, Republic of Korea

† These authors contributed equally to this work.

mixture of L-lactic acid and D-lactic acid, a poly(D, L-lactic) acid which is denoted as PLA, to ensure rapid biodegradation *in vivo*. It is well recognized that PLA composed of D-lactic acid has a more amorphous structure with fewer chain interactions, making it more hydrophilic and therefore more susceptible to hydrolytic cleavage, suggesting that it is highly suitable for bone tissue engineering applications requiring resorption within 8 to 12 months.[19,20] In this study, we fabricated GO-incorporated PLA (GO-PLA) films *via* 3D printing and then examined if they could play an effective role as a potential barrier membrane for guided bone regeneration (GBR) by assessing their feasibility as both *in vitro* culture platforms of preosteoblasts and *in vivo* bone grafts in the rats.

Results & discussion

Physicochemical properties of 3D printed GO-PLA films

The optimum cytocompatible concentration of the GO solution was shown to be 100 $\mu g\ mL^{-1}$ and incorporated into PLA resin to prepare the GO-PLA precursor solution (Fig. 1a, details in the Materials and methods section). The GO-PLA precursor solution was loaded on the 3D printer and 1 (l) × 1 (w) × 0.1 (h) cm^3 constructs were 3D printed (Fig. 1b). The morphology of prepared PLA and GO-PLA films was characterized by field emission scanning electron microscopy (FE-SEM). As depicted in Fig. 1c, the distribution of GO in the PLA resin appeared to be uniform, without any observable aggregation or cracks on the printed constructs. Based on microscopic observation, it can be inferred that the presence of GO did not impede the crosslinking of the PLA solution, which is derived from the hydrophilic nature of the GO particles and their effective dispersion in the solvent. The water contact angle measurements indicated that the contact angle of the GO-PLA film (58.7 ± 0.7°) was significantly lower than that of the PLA film (73.4 ± 3.2°), suggesting that the GO-PLA has a more hydrophilic surface which is more favorable for cell survival and growth (Fig. 1d).[21] These can be attributed to the plenty of hydrophilic functional groups of GO including hydroxyl and epoxide functional groups on its basal planes, and carbonyl and carboxyl groups at the sheet edges. In addition, these hydrophilic moieties of GO facilitate uniform dispersion in the polymer resin due to the strong interactions of polar functional groups in PLA chains.[22] They can also enhance the adhesion between cells and substrates to support the integration of implanted prostheses by regulating the inflammatory responses and connection to immediate tissues.[23]

Raman spectroscopy was conducted on PLA and GO-PLA films for elemental evaluation (Fig. 1e). The characteristic peaks of PLA including 2995 cm^{-1}, 2990 cm^{-1}, and 2878 cm^{-1} denote the stretching vibration of the C–H bond at the PLA plain.[24] The peak of 1762 cm^{-1} represents the stretching vibration of the C=O bond, while peaks of 1447 cm^{-1} and 887 cm^{-1} indicate the asymmetric deformation vibration of the CH_3 bond and stretching vibration of the C–COO bond, respectively.[24,25] On the other hand, different peaks at 1350 cm^{-1}, 1580 cm^{-1}, and 3000 cm^{-1} were observed on the GO-PLA film compared to PLA films (labeled with purple columns). The peaks of 1350 cm^{-1} and 1580 cm^{-1} denote the D
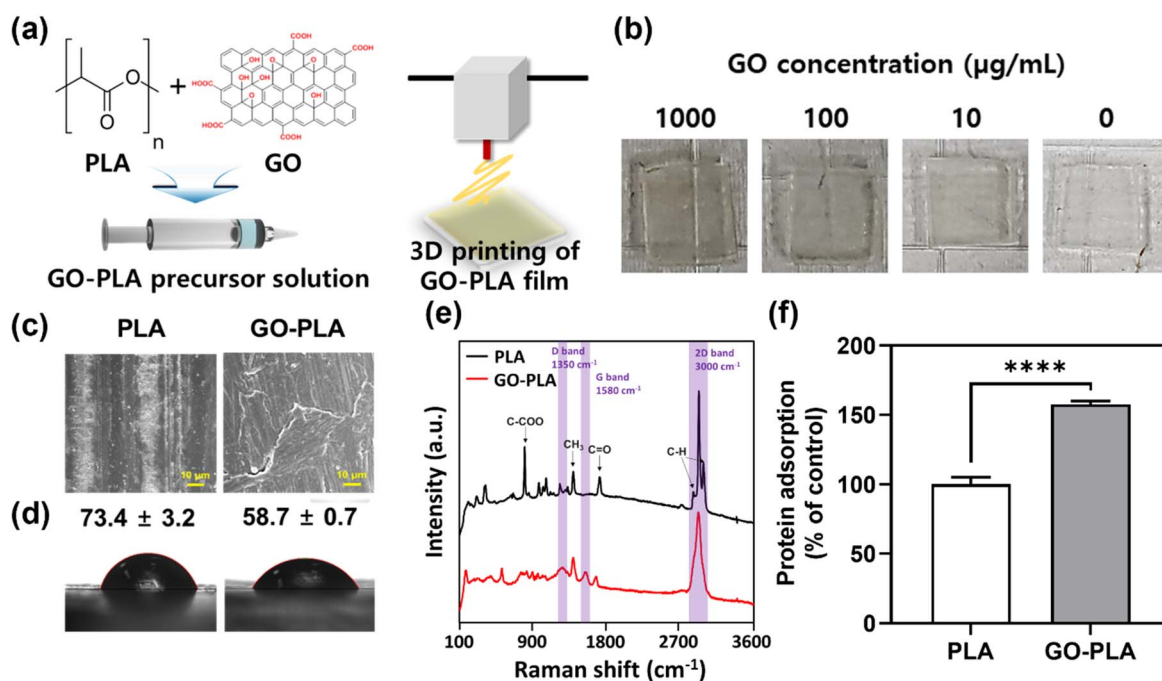
Fig. 1 Physicochemical characterization of 3D printed PLA and GO-PLA films. (a) Schematic diagram of the preparation of the GO-PLA precursor solution and 3D printing of the GO-PLA film. (b) Digital images of 1000, 100, and 10 $\mu g\ mL^{-1}$ GO-containing and intact PLA films. (c) FE-SEM images, (d) water contact angles, (e) Raman spectra, and (f) protein adsorption on PLA and GO-PLA films. The asterisks represent statistical differences (****p < 0.0001).

band and G band, which are specific Raman peaks of graphene materials. Specifically, the intensity ratio of the D band and G band (I_D/I_G) converges to 1.00 suggesting that the GO has maintained its pristine chemical characteristics.[26,27] Moreover, the 2D band peak at 3000 cm^{-1} was slightly shifted compared to the general 2D band of GO, which demonstrates that the incorporated GO is mono-layered.[26] It is critical to properly assess the influence of GO on protein adsorption due to its important role in determining cell–matrix interactions and subsequent cellular behaviours and cytotoxicity. Compared to PLA films, GO-PLA films showed significantly ($p < 0.0001$) enhanced protein adsorption (153%) (Fig. 1f). GO is known to physically bind to proteins with non-covalent self-assembly including weak van der Waals forces, hydrophobic, electrostatic, and π–π stacking interactions, and its enriched functional groups promote covalent bonding with the side groups of amino acid residues located on the protein surfaces.[28] Based on these results, we postulated that the GO-PLA films would anchor the proteins in the serum and support cell growth and osteogenic differentiation.

Cellular behaviours of MC3T3-E1 preosteoblasts on 3D printed GO-PLA films

In vitro cellular behaviours of MC3T3-E1 preosteoblasts on 3D printed PLA and GO-PLA films were evaluated. The cell viability by different GO concentrations in PLA films was assessed by the Cell Counting Kit-8 (CCK-8) assay (Fig. 2a). Compared to PLA films, 10 μg mL^{-1} GO-incorporated PLA films showed rather increased cell viability (113%), while the 100 μg mL^{-1} GO-incorporated PLA films showed slightly decreased cell viability (82%) but were not critically cytotoxic. However, 1000 μg mL^{-1} GO-incorporated PLA films induced appreciable toxicity (55% cell viability) due to the dose-dependent cytotoxicity of GO.[29] Therefore, 100 μg mL^{-1} GO-incorporated PLA films were used for further studies as an optimized concentration.

The potential cytotoxicity of GO-PLA films was assessed including oxidative stress and loss of membrane integrity, which are the most common cytotoxic mechanisms of graphene-based nanomaterials. When the cells were treated with 10 μM H$_2$O$_2$, the green fluorescence of dichlorofluorescein (DCF) was observed indicating intracellular reactive oxygen species (ROS) were generated (Fig. 2b). However, there was no significant expression of DCF on PLA and GO-PLA films suggesting that they do not induce oxidative stress in seeded MC3T3-E1 preosteoblasts. Moreover, there was no significant increase in lactate dehydrogenase (LDH) release on GO-PLA films (105%) compared to PLA films suggesting that the membrane integrity of MC3T3-E1 cells was not broken on GO-PLA films (Fig. 2c). The initial adhesion of MC3T3-E1 cells was significantly ($p < 0.0001$) increased on GO-PLA films (125%) compared to PLA films (Fig. 2d). During 48 h of incubation, the migration speed of MC3T3-E1 cells was retained faster (2.31–1.08-fold) on GO-PLA films at every time point compared to PLA films (Fig. 2e). Subsequently, the cell proliferation rate was significantly ($p < 0.0001$) increased on GO-PLA films (134, 127, and 128% at 1, 3, and 5 days, respectively) compared to PLA
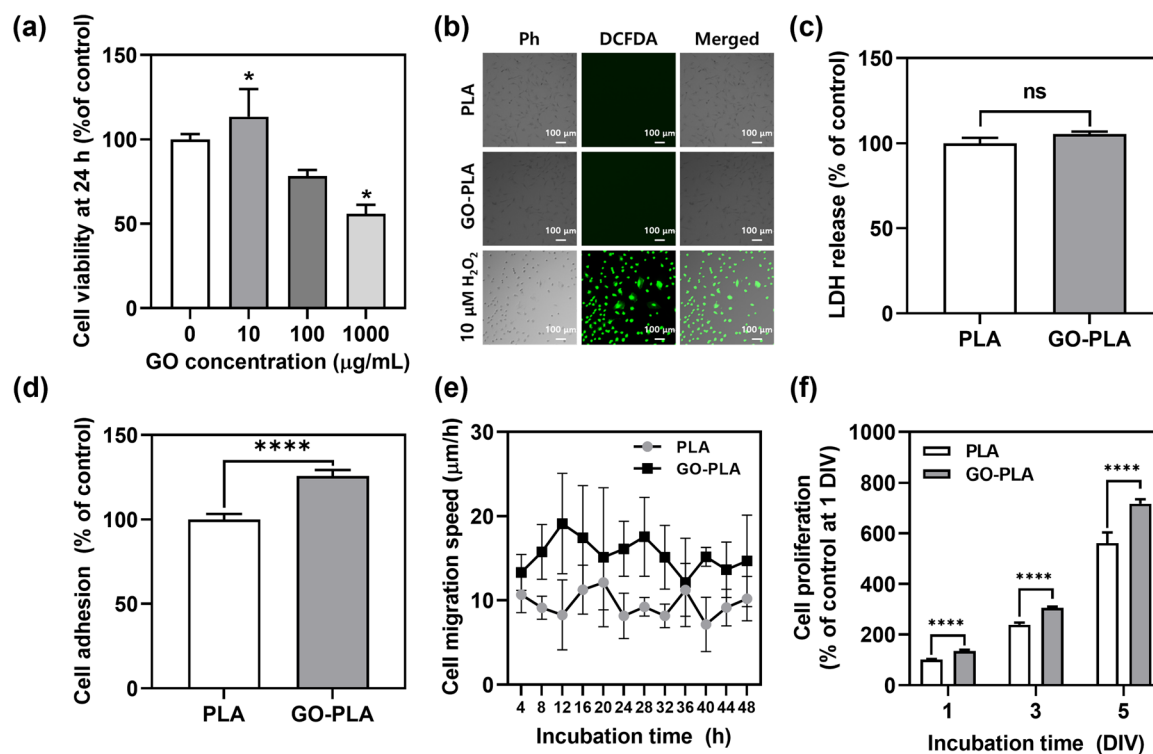

Fig. 2 Cellular behaviours of MC3T3-E1 preosteoblasts cultured on 3D printed PLA and GO-PLA films. (a) Cell viability of MC3T3-E1 preosteoblasts on 10, 100, and 1000 μg mL^{-1} GO-incorporated or pristine PLA films at 24 h, (b) intracellular ROS generation at 24 h, (c) LDH release at 24 h, (d) initial cell adhesion at 6 h, (e) cell migration speed during 48 h, and (f) cell proliferation profiles for 5 DIV. Ph indicates phase contrast. Scale bars of (b) represent 100 μm. The asterisks represent statistical differences (*$p < 0.05$ and ****$p < 0.0001$).

films at the same days (Fig. 2f). These results indicate that the incorporation of GO into PLA films can promote robust cellular behaviours by supporting initial cell adhesion, migration, and proliferation.

A live/dead assay was conducted to assess the cell viability. Due to the proliferation-promoting effects of GO, MC3T3-E1 cells on GO-PLA films showed increased confluency compared to PLA films (Fig. 3a). In both 24 and 48 h, most of the cells on GO-PLA were viable which is comparable to those on PLA films suggesting that the incorporated GO did not hinder the viability of MC3T3-E1 preosteoblasts (Fig. 3b and c). After 5 days of culture, cells were fully proliferated on PLA and GO-PLA films showing typical mesh-like morphology of MC3T3-E1 preosteoblasts (Fig. 3d). The F-actin spreading area and the number of nuclei of cells on GO-PLA films (107 and 109% compared to control, respectively) were comparable to those on PLA films suggesting that the GO-PLA did not induce any harmful effects on MC3T3-E1 preosteoblast growth (Fig. 3e and f).

It is important to maintain high viability and active proliferation of cells to promote successful osseointegration of the implant prostheses. Graphene materials have been suggested as the gold standard for orthopedic and dental implants due to their excellent biofunctionality and osteogenic capability.[30–32] The intrinsic mechanisms of cell–nanomaterial interactions between GO and MC3T3-E1 preosteoblasts can be explained as biomolecular interactions, electrical properties, topography, and local stiffness.[33] The biomolecular interaction of GO represents its capacity to anchor proteins, growth factors, and biomolecules through physical adsorption and chemical interactions. Furthermore, the electrostatic repulsion could produce higher adsorption of ECM proteins (*e.g.* fibronectin, laminin, and vitronectin) and direct linkage between the cellular receptors and the film surfaces, which support cellular attachment on the substrate and modulation of cellular growth.[34]

The majority of these effects stem from plenty of functional groups present on the basal plane and edges of GO, including epoxy, carbonyl, carboxyl, and hydroxyl groups. Epoxy groups directly engage in chemical reactions with sulfhydryl, amino, and carboxyl groups, resulting in the formation of strong covalent bonds with several biomolecules.[35] The carbonyl and
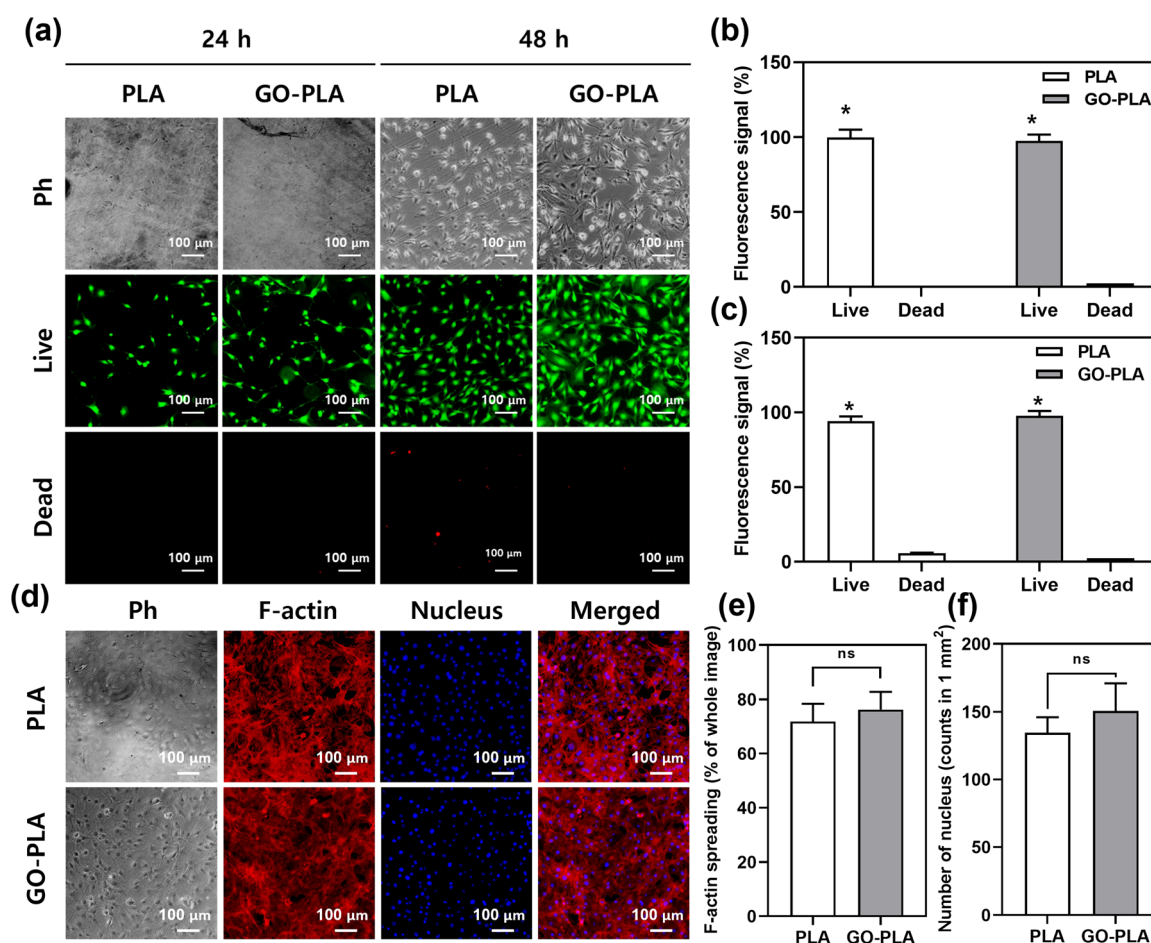
Fig. 3 Live/dead assay and immunocytochemical analysis to observe cell viability and cellular morphology of MC3T3-E1 preosteoblasts cultured on 3D printed PLA and GO-PLA films. (a) Fluorescence micrographs and their quantification at (b) 24 h and (c) 48 h. (d) Immunofluorescence staining of cells at 5 DIV. TRITC (red) and DAPI (blue) denote F-actin and nucleus, respectively. Ph indicates phase contrast. (e) F-actin spreading area and (f) the number of the nucleus quantified based on images of (d). Scale bars of (a) and (d) represent 100 μm. The asterisk represents statistical difference (*$p < 0.05$).

carboxyl groups also participate in chemical reactions with amino acids such as lysine and arginine in proteins, leading to the creation of stable covalent bonds that aid in the immobilization of proteins on the surface of GO.[36] Additionally, the hydroxyl group not only enhances the interaction with polymer chains but also improves the stability and biocompatibility of the composites by facilitating hydrogen bonding with water

molecules.[37,38] The hydrophilic nature of GO can lead to improved focal adhesion formation which is comparable to the native environment.[39] Moreover, the surface topography and stiffness act as biophysical cues that can promote different cell anchorage and mechanosensitive pathways, which produce cellular cytoskeleton rearrangement and trigger a cascade of transduction signals that modulate cell phenotypes.[40,41]
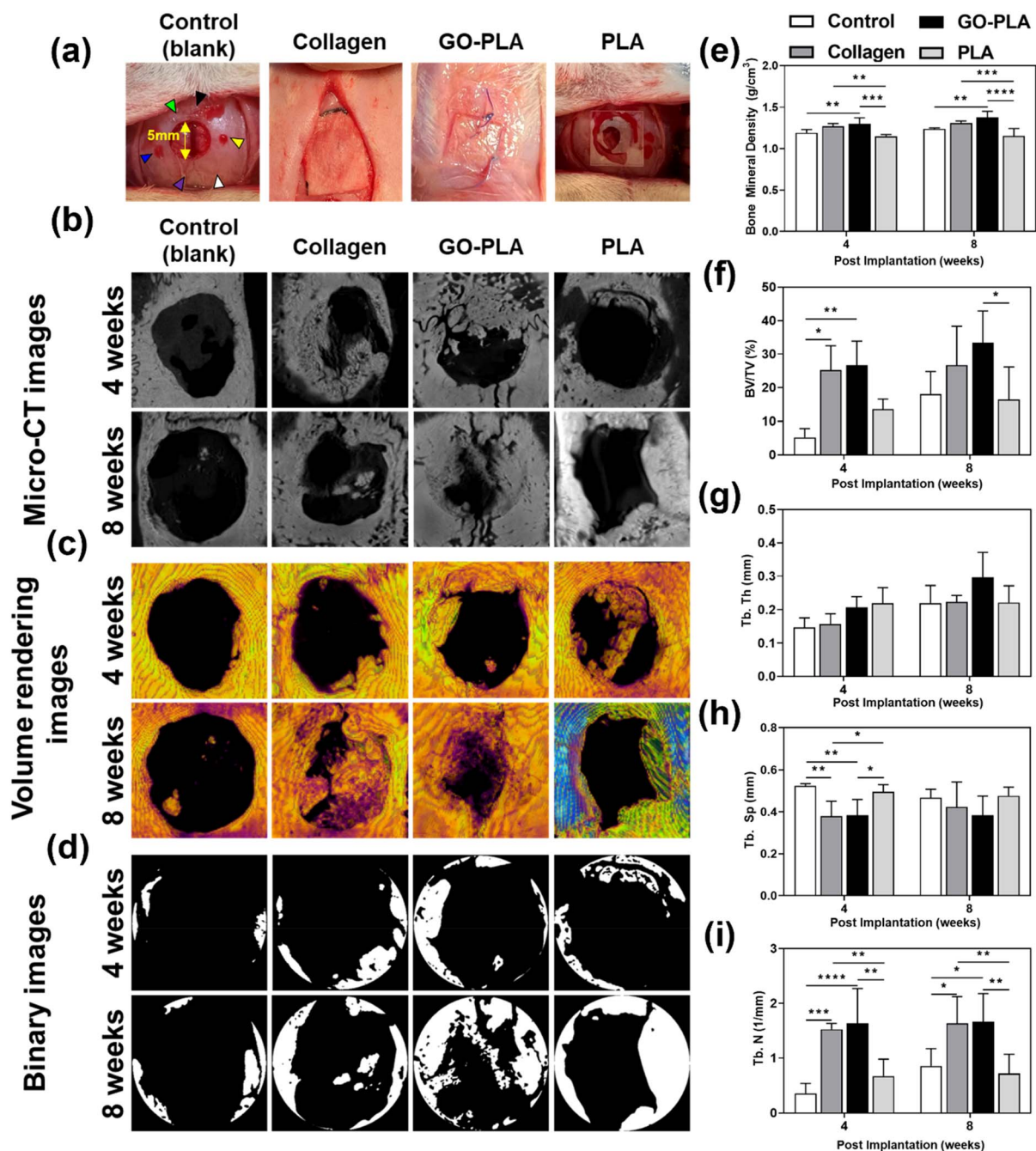

Fig. 4 Images and statistical results of the calvarial defect model with/without films using micro-CT analysis. (a) Digital images of film implantation on calvarial bone defect models. Each arrowhead indicates as follows, green: coronal suture, black: bregma, blue: left lateral parietal bone, purple: lambda, yellow: right lateral parietal bone, and white: lambdoid suture. (b) Micro-CT images, (c) volume rendering images, and (d) binary images according to micro-CT analysis. Bone healing on the films were statistically evaluated for (e) BMD, (f) BV/TV, (g) Tb.Th, (h) Tb.Sp, and (i) Tb.N. The asterisks represent statistical differences (*$p < 0.05$, **$p < 0.01$, ***$p < 0.001$, and ****$p < 0.0001$).

Osteogenic effects of 3D printed GO-PLA membranes in rat calvarial defect models

The calvarial defect site was set in the volume of interest (VOI) and bone mineral density (BMD), trabecular bone volume to total volume fraction (BV/TV), trabecular thickness (Tb.Th), trabecular number (Tb.N), and trabecular separation (Tb.Sp) were quantitatively analyzed to evaluate the efficacy of osteogenesis (Fig. 4a). Fig. 4b–d show computed tomography (CT) images derived from micro-CT, volume rendering images, and binary images for each group. The BMD results showed similar trends at 4 and 8 weeks (Fig. 4e). At 4 weeks, the GO-PLA membranes (1.30 ± 0.07 g cm^{-3}) showed significantly higher BMD than the control (1.19 ± 0.04 g cm^{-3}) and PLA (1.14 ± 0.02 g cm^{-3}) membranes ($p < 0.01$ and $p < 0.001$, respectively). The BMD of the collagen membrane (1.27 ± 0.03 g cm^{-3}) was also significantly greater than that of the PLA membrane ($p < 0.01$). In the results at 8 weeks, the BMD of the GO-PLA membrane (1.38 ± 0.06 g cm^{-3}) was significantly higher than that of the control (1.24 ± 0.01 g cm^{-3}) and PLA (1.16 ± 0.08 g cm^{-3}) membranes ($p < 0.01$ and $p < 0.0001$, respectively). The collagen membrane (1.31 ± 0.02 g cm^{-3}) also exhibited a significantly greater value than the PLA membrane ($p < 0.001$). On the other hand, there was no significant difference between the GO-PLA and collagen membranes at 4 and 8 weeks. In the BV/TV results at 4 weeks (Fig. 4f), the collagen ($25.25 \pm 6.62\%$) and GO-PLA ($26.70 \pm 6.55\%$) membranes exhibited a significantly higher value than the control ($5.23 \pm 2.38\%$) group ($p < 0.05$ and $p < 0.01$, respectively). There was no significant difference between the PLA ($13.60 \pm 2.67\%$), GO-PLA and collagen membranes. Similar to the results at 4 weeks, there was no significant difference between the GO-PLA ($33.35 \pm 8.70\%$) and collagen ($26.77 \pm 10.58\%$) membranes at 8 weeks. Moreover, the GO-PLA membrane showed a significantly higher BV/TV value compared to the PLA membrane ($16.44 \pm 8.90\%$, $p < 0.05$). Based on our results, it could be identified that the GO-PLA membrane enables higher bone density and bone formation volume than the PLA membrane, and it shows performance similar to or even higher than that of the widely used collagen membrane. In the results of the Tb.Th, there was no significant difference among all groups at both 4 and 8 weeks (Fig. 4g). At 4 weeks, the Tb.Th result was highest in the order of the PLA (0.22 ± 0.04 mm), GO-PLA (0.21 ± 0.05 mm), collagen (0.16 ± 0.03 mm), and control (0.15 ± 0.03 mm) membranes. In contrast, the Tb.Th value at 8 weeks was highest in the order of GO-PLA (0.30 ± 0.07 mm), collagen (0.22 ± 0.02 mm), PLA (0.22 ± 0.05 mm), and control (0.22 ± 0.05 mm) membranes. The results of the GO-PLA membrane showed similar or higher values than the other groups. At 4 weeks, the Tb.Sp of the GO-PLA membrane (0.38 ± 0.07 mm) was significantly lower than that of the control (0.52 ± 0.01 mm) and PLA (0.50 ± 0.03 mm) membranes ($p < 0.01$ and $p < 0.05$, respectively, Fig. 4h). The collagen membrane (0.38 ± 0.07 mm) showed the same Tb.Sp value as the GO-PLA membrane. However, there was no significant difference among all groups at 8 weeks. In the results of the Tb.N at 4 weeks (Fig. 4i), the GO-PLA membrane (1.64 ± 0.58 mm^{-1}) exhibited significantly higher values than the control ($0.36 \pm$

0.17 mm^{-1}) and PLA (0.67 ± 0.27 mm^{-1}) membranes ($p < 0.0001$ and $p < 0.01$, respectively). The Tb.N of the collagen membrane (1.53 ± 0.10 mm^{-1}) was significantly greater than those of the control and PLA membranes ($p < 0.001$ and $p < 0.01$, respectively). At 8 weeks, the GO-PLA membrane (1.66 ± 0.46 mm^{-1}) displayed a significantly higher Tb.N value than the control (0.86 ± 0.29 mm^{-1}) and PLA (0.72 ± 0.32 mm^{-1}) membranes ($p < 0.05$ and $p < 0.01$, respectively). The collagen membrane (1.63 ± 0.45 mm^{-1}) showed similar results to the GO-PLA membrane and there was no significant difference between both groups. The previous studies reported that osteoporosis models are shown to have lower Tb.N and less bone connectivity and that bone density increases as the Tb.N increases and the Tb.Sp decreases.[42–46] Similar to the results of previous studies, our results confirmed that the GO-PLA membrane had the highest Tb.N and the lowest Tb.Sp compared to the other groups. In addition, the BMD of the GO-PLA membrane was significantly higher than that of the other groups. Therefore, it is considered that the GO-PLA membrane possesses the potential to promote osseointegration, bone connectivity, and initial stability.

Recent studies have shown that graphene-based scaffolds have excellent potential for *in vivo* GBR. Wang *et al.* demonstrated that polycaprolactone/graphene scaffolds transplanted in rat calvarial defects have bone remodelling capability.[47] Owing to the low immunogenicity of graphene materials, lower expression of tumor necrosis factor α (TNF-α) and interleukin 1 β (IL-1β) was observed. In particular, the application of external microcurrent along with graphene materials demonstrated remarkable osteoconductivity, resulting in the formation of well-structured new bone tissues. This process was accompanied by an increase in the expression of ALP and osteoprotegerin (OPG), while the expression of receptor activator of NF-κB (RANK) and RANK ligand (RANKL) was down-regulated. RANKL/RANK signaling regulates osteoclast development, activation, and viability during normal bone modeling and remodeling. OPG serves to safeguard against excessive bone resorption by binding to RANKL and inhibiting its interaction with RANK, implying that graphene exhibits inhibitory effects on osteoclast activity.[48] Wang *et al.* introduced GO-coated microgrooved Ti–6Al–4V alloy implants and evaluated their osseointegration in rabbit femur bone.[49] Micro-CT and histological analysis showed that GO coating and microgroove significantly enhanced new apatite formation and bone-implant contact area. Additionally, the antimicrobial properties of graphene materials have the potential to be advantageous in the clinical translation of graphene-functionalized scaffolds. Mazinani *et al.* implemented a GO coating layer on plasma electrolytic oxidized titanium implants to endow them with antibacterial properties.[50] The GO layer not only facilitated increased protein adsorption in simulated body fluid (SBF) but also effectively hindered the growth of *E. coli* (approximately 80%) and *S. aureus* (100%), demonstrating its exceptional antibacterial properties. Besides, previously reported studies have emphasized that GO can induce osteogenic genes in dental pulp stem cell by regulating osteogenic gene expression, macrophage polarization, and inflammation.[51,52] Along with these previous

Conclusions

In conclusion, we developed GO-PLA films, produced simply by the 3D printing process to evaluate their potential in GBR. As designed in our scheme, the incorporation of GO in PLA films exhibited excellent physicochemical properties and enhanced protein adsorption, which can provide favorable microenvironments to facilitate the cellular behaviours of MC3T3-E1 preosteoblasts. The results indicated that the initial cell adhesion, migration rate, and proliferation rate of MC3T3-E1 cells were notably increased on GO-PLA films while maintaining high cell viability and normal morphology. Furthermore, GO-PLA films exhibited exceptional osteogenic activity in rat calvarial defect models that led to explicitly spontaneous osteogenic differentiation and rapid osseointegration *in vivo*. As an on-demand concept, our strategy on the potential use of the GO-PLA films is of paramount importance by directing cellular responses and behaviours in the context of the development of biofunctional 2D nanomaterials to promote bone regeneration. Taken together, our observations on this functional nano-biomaterial suggest that the combination of GO and PLA can be a promising candidate for GBR membranes, extending to other types of cells or tissues that provide an amicable matrix to find critical signaling pathways toward cellular behaviours as well as accelerating osteogenesis. However, a more detailed mechanism of osteogenic activity of GO-PLA films, involving intracellular signaling pathways, is yet obscure and requires further study at molecular levels to fully understand it. In any case, we envision that our 3D printed membranes incorporated with GO would be potential candidates for the development of implantable devices, such as GBR and joints because they possess excellent biocompatibility and bioactivity.

Materials and methods

Materials and apparatus

Acetone, α-Minimum Essential Medium (αMEM), antibiotic-antimycotic solution, bovine serum albumin (BSA), chloral hydrate, 4′,6-diamidino-2-phenylindole (DAPI), Dulbecco's phosphate-buffered saline (DPBS), fetal bovine serum (FBS), formaldehyde, isopropyl alcohol (IPA), and Triton X-100 were purchased from Sigma-Aldrich (St. Louis, MO). Pierce bicinchoninic acid (BCA) protein and live/dead assay kits and 6-chloromethyl-2′,7′-dichlorofluorescein diacetate (CM-H$_2$DCFDA) were purchased from ThermoFisher Scientific (Waltham, MA). CCK-8 and LDH assay kits were purchased from Dojindo (Kumamoto, Japan) and Takara Bio Inc. (Shiga, Japan), respectively. GO and tetramethylrhodamine (TRITC)-labeled phalloidin were purchased from Graphene Laboratories Inc. (Ronkonkoma, NY) and Molecular Probes Inc. (Eugene, OR), respectively. Pentobarbital, povidone-iodine alcohol, and Surgifit products (4-0) were purchased from Hanlim Pharm, Co., Ltd (Gyeonggi, Republic of Korea), Green Pharmaceutical Co., Ltd (Seoul, Republic of Korea), and Ailee Co., Ltd (Busan, Republic of Korea), respectively. PLA (50 : 50 poly(D, L-lactide) acid) resin was kindly provided by 3DMaterials Co., Ltd (Anyang, Republic of Korea). Collagen films were purchased from Geistlich Pharma AG (Bio-Gide, Wolhusen, Switzerland).

CHITUBOX V1.9.0 software (Phrozen, Hsinchu City, Taiwan) was used to prepare STL files, printed by an extrusion-based 3D printer (Phrozen Sonic Mini 8K), and crosslinked by post-crosslinking equipment (LuDent Cure L, 3DMaterials Co., Ltd). Physicochemical characterization was performed by FE-SEM (Carl Zeiss Supra 40VP, Oberkochen, Germany), Raman spectroscopy (UniNanoTech Co., Ltd, Yongin, Republic of Korea), and contact angle measurements (SmartDrop, Femtofab Co., Ltd, Seongnam, Republic of Korea). For cell analysis, absorbance was measured using a microplate reader (Varioskan LUX, ThermoFisher Scientific), fluorescence microscopy using a fluorescence microscope (IX81-F72, Olympus Optical Co., Ltd, Osaka, Japan), live cell imaging using a DP74 camera (Olympus Optical, Co., Ltd), and quantification using ImageJ software (National Institute of Health, Bethesda, MD). For *in vivo* analysis, micro-CT was captured using a high-resolution Skyscan 1273 (Bruker, Kontich, Belgium) and analyzed using a CT Analyser v.1.18.4.0 (CTAn, Bruker, Kontich, Belgium).

3D printing of GO-PLA films

The hydroxyl groups of PLA pre-polymers (62 w/v% in ethyl acetate) were reacted with 2-isocyanatoethyl methacrylate to synthesize ultraviolet (UV)-crosslinkable methacrylated PLA. A mixture of 3 w/v% of benzoyl-diphenyl-phosphineoxide (TPO) and 1-hydroxy cyclohexyl phenyl methanone (CP-4) was introduced to prepare the PLA resin. 4000 μg mL^{-1} GO solution (diluted in deionized water) was homogeneously mixed with photo-crosslinkable PLA resins to prepare the GO-PLA precursor solution. The 1 (l) × 1 (w) × 0.1 (h) cm^3 3D models were prepared as STL files using 50 μm slices. Before 3D printing, the GO-PLA precursor solution was sonicated for 2 h and gently vortexed to avoid precipitation. The GO-PLA precursor solution was loaded on a 3D printer and printed with 405 nm UV exposure for 8.5 s on every layer using the optimized printing parameters. Subsequently, the printed constructs were sonicated in IPA to detach the impurities and maintained at 25 °C for 1 min. For the post-crosslinking, 405 nm UV light was radiated by post-crosslinking equipment. The prepared GO-PLA samples were washed with DPBS three times and maintained under 405 nm UV radiation overnight for sterilization.

Physicochemical characterization of 3D printed GO-PLA films

3D printed PLA and GO-PLA films were washed with acetone and DPBS three times respectively and dried at 25 °C for every experiment in this section. The surface morphologies of PLA and GO-PLA films were imaged by FE-SEM at an accelerating voltage of 15 kV. The elemental compositions of PLA and GO-PLA films were characterized by Raman spectroscopy with 532 nm laser excitation. The water contact angles of PLA and GO-PLA films were measured by the sessile drop method using a contact angle measurement system. A 1 μL sessile drop of distilled water was formed on all the matrices. To investigate

the amounts of protein adsorption on surfaces, PLA and GO-PLA films were placed in a 48-well plate, soaked with 1 mL FBS, and incubated at 37 °C for 24 h. Subsequently, the supernatants were removed, washed with DPBS three times, and the amounts of protein adsorbed on PLA and GO-PLA film surfaces were assessed using a BCA assay kit, a copper-based protein quantification kit, following the manufacturer's protocol.

Cell culture and conditions

A murine preosteoblastic cell line (MC3T3-E1 preosteoblasts from C57BL/6 mouse calvaria) was purchased from the American Type Culture Collection (ATCC, Rockville, MD). The cells were routinely cultured in αMEM supplemented with 10% FBS and 1% antibiotic-antimycotic solution (including 10 000 U penicillin, 10 mg streptomycin, and 25 μg amphotericin B per mL) at 37 °C in a humidified atmosphere of 5% CO_2. At approximately 80% confluency, the cells were subcultured and media were changed every 48 h. The 2 or 3 passages after thawing were utilized for *in vitro* cell experiments.

Examination of cellular behaviours on 3D printed GO-PLA films

Between every procedure noted in this section, films were washed with sterilized DPBS one to three times to remove residues. The cell viability of MC3T3-E1 preosteoblasts on the 3D printed PLA films incorporating the different concentrations (10, 100, and 1000 μg mL^{-1}) of GO was assessed by the CCK-8 assay. The cells were seeded on the PLA and GO-PLA films at an initial density of 5×10^4 cells per film and then incubated in a CO_2 incubator for 24 h. After the removal of media, the cells were reacted with the CCK-8 assay solution (diluted in DPBS at 1 : 9 v/v) for 2 h. Subsequently, 100 μL of supernatants were transferred to 96-well plates and the absorbance was measured at 450 nm using a microplate reader. For the cell adhesion test, 10^4 cells in 10 μL suspensions were spot-seeded on the PLA and GO-PLA films, and then examined after 6 h by the CCK-8 assay. Based on the results of the viability measurement, the optimum concentration of GO in PLA films was fixed to 100 μg mL^{-1} for the following experiments. For the cell proliferation test, 10^4 cells were seeded on the PLA and GO-PLA films, and then examined by the CCK-8 assay after 1, 3, and 5 days *in vitro* (DIV). Both cell adhesion and proliferation were determined with the same protocol as described above.

For the LDH assay, after 24 h incubation of MC3T3-E1 preosteoblasts on PLA films with or without 100 μg mL^{-1} GO at an initial density of 5×10^4 cells per film, the supernatant from the cultured cells was transferred to a new 96-well plate. Afterward, an LDH assay solution was added to each well and then incubated for 30 min at 25 °C in the dark. The absorbance was measured at 490 nm using a microplate reader. Cellular oxidative stress on PLA films with or without 100 μg mL^{-1} GO was evaluated by measuring intracellular ROS generation using a CM-H$_2$DCFDA kit. The cells were seeded on PLA and GO-PLA films at the same density as described above and then incubated for 24 h. 10 μM H_2O_2 was treated for 1 h to generate ROS as a positive control. Subsequently, 5 μM DCFDA solution was

added and reacted for 30 min in a CO_2 incubator. Fluorescence micrographs were captured and the degree of fluorescence was quantified using ImageJ software. Cell migration was assessed by live cell imaging. Initially, the cells were seeded on PLA and GO-PLA films at an initial density of 10^3 cells per film and then maintained in a transparent mini-CO_2 incubator for *in situ* optical imaging. The images were captured using a DP74 camera attached to the fluorescence microscope at 3 min time intervals for 48 h. Ten individual cells were manually tracked using ImageJ software and the average migration speed every 4 h was calculated.

Live/dead assay and immunocytochemical analysis

At 24 h and 48 h of incubation on PLA films with or without 100 μg mL^{-1} GO, the MC3T3-E1 preosteoblasts were treated with a live/dead assay solution (2 μM calcein AM and 4 μM ethidium homodimer-1) for 30 min in a CO_2 incubator. The stained cells were rinsed three times with DPBS and imaged by fluorescence microscopy. The resulting fluorescence images were quantified using ImageJ software. To observe the alteration of cellular morphologies on PLA and GO-PLA films, immunofluorescence staining was performed at 5 DIV. After the removal of the culture medium, 3.7% formaldehyde solution was added for 10 min for fixation. 0.1% Triton X-100 was treated for 5 min to permeabilize the cells on each film, followed by blocking with 2% BSA for 30 min to prevent the non-specific binding. Subsequently, 165 nM TRITC-labelled phalloidin and 300 nM DAPI were added and incubated for 30 min at 25 °C in the dark. Fluorescence images were obtained using a fluorescence microscope. The F-actin spreading and the number of the nucleus were quantified using ImageJ software.

Preparation of animals

All animal experiments were conducted in accordance with the Animal Research: Reporting of *In Vivo* Experiments (ARRIVE) guidelines. Twenty-four 6 weeks-old female Sprague Dawley rats (150–200 g, Orient Bio, Gapyeong, Republic of Korea) were used. The rat room conditions in the Specific Pathogen-Free (SPF) laboratory maintained a temperature of 21 °C ± 1 °C, 55% humidity, and a 12 h light/12 h dark cycle (light: 07:30–20:00, dark: 20:00–07:30). The rats were supplied with normal feed (Purina Rodent Chow, Purina Co., Ltd, Seoul, Republic of Korea) and water. The health status of the rats used in this study was checked, and their weights were measured. The rat calvarial defects were formed and randomized to a control group without films or treatment groups with PLA and GO-PLA films. The control of this experiment was a collagen film, which is an optimal absorbent membrane according to mechanical testing[53] and histomorphometric analysis.[54] Six rats were used per group.

Surgical procedures

Before surgery, all animals used in this study were allowed to acclimatize to the rat room conditions for 1 week. The rats were anesthetized with intraperitoneal injection using a 3 mL mixture (100 mg kg^{-1}) of pentobarbital and chloral hydrate. The

calvarial skin at the surgical site was shaved and disinfected with povidone-iodine alcohol. After exposing the scalp and parietal bone by making a sagittal incision in the midline region, both the external and internal corticals were removed while preserving the dura mater. The calvarial defect with a diameter of 5 mm was formed in the center of the skull using a 5 mm diameter trephine bur.[55] In order to form the calvarial defect, a dental drill handpiece was drilled at 1500 revolutions per minute (rpm) and cooled using normal saline. The periosteum and skin were sutured using Surgifit products.

Micro-CT scanning

All experimental groups were sacrificed at 4 and 8 weeks after surgery, respectively. A square region (7 mm in width × 7 mm in height) of the skull was extracted from the rats sacrificed in each group and all specimens were fixed in 3.7% formaldehyde solution for 72 h. Test blocks in each group were performed by the micro-CT. All specimens were scanned under the same conditions (90 kV, 166 μA, and an isotropic resolution of 11.9 μm), which took about 45 minutes per specimen. Approximately 700 micro-CT images were generated and analyzed using a CT Analyser.[56] The variables such as bone mineral density (BMD), trabecular bone volume to total volume fraction (BV/TV), trabecular thickness (Tb.Th), trabecular number (Tb.N), and trabecular separation (Tb.Sp) were measured and evaluated to compare between groups (control, collagen, GO-PLA, and PLA).

Statistical analysis

All variables were tested in three independent cultures for each experiment, which was repeated twice ($n = 6$). The quantitative data are expressed as the mean ± standard deviation. Before statistical analysis, the data were analysed for the equality of variances using Levene's test. Multiple statistical comparisons were performed using the Bonferroni test after a preliminary one-way analysis of variance; the asterisks (* to ****) indicate statistical significance between groups (*$p < 0.05$, **$p < 0.01$, ***$p < 0.001$, ****$p < 0.0001$, and 'ns': not significant).

Author contributions

H. J. Jang and M. S. Kang: writing – original draft preparation, investigation, data curation. W. –H. Kim, H. J. Jo, and S. –H. Lee: investigation, visualization. E. J. Hahm, J. H. Oh, and S. W. Hong: formal analysis, validation. B. Kim and D. –W. Han: conceptualization, funding acquisition, project administration, supervision, writing – review & editing.

Conflicts of interest

There are no conflicts to declare.

Acknowledgements

References

1 M. Ansari, *Prog. Biomater.*, 2019, **8**, 223–237.

2 I. S. Raja, M. S. Kang, S. W. Hong, H. Bae, B. Kim, Y.-S. Hwang, J. M. Cha and D.-W. Han, *Int. J. Bioprint.*, 2022, **9**, 635.

3 H. Qu, H. Fu, Z. Han and Y. Sun, *RSC Adv.*, 2019, **9**, 26252–26262.

4 M. M. Stevens, *Mater. Today*, 2008, **11**, 18–25.

5 M. S. Kang, J. H. Lee, S. W. Hong, J. H. Lee and D.-W. Han, *J. Compos. Sci.*, 2021, **5**, 23.

6 Y. C. Shin, J.-H. Bae, J. H. Lee, I. S. Raja, M. S. Kang, B. Kim, S. W. Hong, J.-B. Huh and D.-W. Han, *Biomater. Res.*, 2022, **26**, 11.

7 M. S. Kang, J. I. Kang, P. Le Thi, K. M. Park, S. W. Hong, Y. S. Choi, D.-W. Han and K. D. Park, *ACS Macro Lett.*, 2021, **10**, 426–432.

8 M. N. Collins, G. Ren, K. Young, S. Pina, R. L. Reis and J. M. Oliveira, *Adv. Funct. Mater.*, 2021, **31**, 2010609.

9 Z.-K. Cui, S. Kim, J. J. Baljon, B. M. Wu, T. Aghaloo and M. Lee, *Nat. Commun.*, 2019, **10**, 3523.

10 S. Bose, S. Vahabzadeh and A. Bandyopadhyay, *Mater. Today*, 2013, **16**, 496–504.

11 M. Monavari, S. Homaeigohar, M. Fuentes-Chandia, Q. Nawaz, M. Monavari, A. Venkatraman and A. R. Boccaccini, *Mater. Sci. Eng., C*, 2021, **131**, 112470.

12 C. Hu, Z. Chen, L. Tang, J. Liu, J. Yang, W.-F. Lai, T. Wu, S. Liao, X. Zhang and H. Pan, *Mater. Des.*, 2022, **216**, 110551.

13 I. S. Raja, H. J. Jang, M. S. Kang, K. S. Kim, Y. S. Choi, J.-R. Jeon, J. H. Lee and D.-W. Han, *Adv. Exp. Med. Biol.*, 2022, **1351**, 89–105.

14 S. A. Aguila, D. Shimomoto, F. Ipinza, Z. I. Bedolla-Valdez, J. Romo-Herrera, O. E. Contreras, M. H. Farías and G. Alonso-Núñez, *Sci. Technol. Adv. Mater.*, 2015, **16**, 055004.

15 S. Chung, R. A. Revia and M. Zhang, *Adv. Mater.*, 2021, **33**, 1904362.

16 S. Song, H. Shen, Y. Wang, X. Chu, J. Xie, N. Zhou and J. Shen, *Colloids Surf., B*, 2020, **185**, 110596.

17 C. A. Tannoury and H. S. An, *Spine*, 2014, **14**, 552–559.

18 S. Liu, S. Qin, M. He, D. Zhou, Q. Qin and H. Wang, *Composites, Part B*, 2020, **199**, 108238.

19 X. Qi, Y. Ren and X. Wang, *Int. Biodeterior. Biodegrad.*, 2017, **117**, 215–223.

20 S. Wei, J.-X. Ma, L. Xu, X.-S. Gu and X.-L. Ma, *Mil. Med. Res.*, 2020, **7**, 54.

21 M. S. Kang, S. J. Jeong, S. H. Lee, B. Kim, S. W. Hong, J. H. Lee and D.-W. Han, *Biomater. Res.*, 2021, **25**, 4.

22 T. Hwang, J.-S. Oh, W. Yim, J.-D. Nam, C. Bae, H.-i. Kim and K. J. Kim, *Sep. Purif. Technol.*, 2016, **166**, 41–47.

23 M. Ferrari, F. Cirisano and M. C. Morán, *Colloids Interfaces*, 2019, **3**, 48.

24 A. M. Pandele, A. Constantinescu, I. C. Radu, F. Miculescu, S. Ioan Voicu and L. T. Ciocan, *Materials*, 2020, **13**, 274.

25 W. Jia, Y. Luo, J. Yu, B. Liu, M. Hu, L. Chai and C. Wang, *Opt. Express*, 2015, **23**, 26932–26939.

26 B. Tang, H. Guoxin and H. Gao, *Appl. Spectrosc. Rev.*, 2010, **45**, 369–407.

27 A. C. Ferrari and D. M. Basko, *Nat. Nanotechnol.*, 2013, **8**, 235–246.

28 M. C. Shin, M. S. Kang, R. Park, S. Y. Chae, D.-W. Han and S. W. Hong, *Appl. Surf. Sci.*, 2021, **561**, 150115.

29 I. S. Raja, J. H. Lee, S. W. Hong, D.-M. Shin, J. H. Lee and D.-W. Han, *J. Hazard. Mater.*, 2021, **409**, 124915.

30 K. O. Park, J. H. Lee, J. H. Park, Y. C. Shin, J. B. Huh, J.-H. Bae, S. H. Kang, S. W. Hong, B. Kim and D. J. Yang, *Appl. Spectrosc. Rev.*, 2016, **51**, 540–551.

31 J. H. Lee, Y. C. Shin, S.-M. Lee, O. S. Jin, S. H. Kang, S. W. Hong, C.-M. Jeong, J. B. Huh and D.-W. Han, *Sci. Rep.*, 2015, **5**, 18833.

32 M. S. Kang, H. J. Jang, S. H. Lee, Y. C. Shin, S. W. Hong, J. H. Lee, B. Kim and D.-W. Han, *Adv. Exp. Med. Biol.*, 2022, **1351**, 65–87.

33 J. M. Kwak, J. Kim, C. S. Lee, I. S. Park, M. Lee, D. H. Min and I. S. L. Yeo, *Adv. Mater. Interfaces*, 2022, **9**, 2201116.

34 S. Kumar and S. H. Parekh, *Commun. Chem.*, 2020, **3**, 8.

35 C. Tyagi, L. K. Tomar and H. Singh, *J. Appl. Polym. Sci.*, 2009, **111**, 1381–1390.

36 W. Zhou, W. Zhuang, L. Ge, Z. Wang, J. Wu, H. Niu, D. Liu, C. Zhu, Y. Chen and H. Ying, *J. Colloid Interface Sci.*, 2019, **546**, 211–220.

37 S. Gautam, S. Sharma, B. Sharma and P. Jain, *Polym. Compos.*, 2021, **42**, 2829–2837.

38 Y. Y. Khine, X. Wen, X. Jin, T. Foller and R. Joshi, *Phys. Chem. Chem. Phys.*, 2022, **24**, 26337–26355.

39 S. H. Kang, Y. C. Shin, E. Y. Hwang, J. H. Lee, C.-S. Kim, Z. Lin, S. H. Hur, D.-W. Han and S. W. Hong, *Mater. Horiz.*, 2019, **6**, 1066–1079.

40 P. c. C. Henriques, A. T. Pereira, A. L. Pires, A. M. Pereira, F. D. Magalhães and I. s. C. Gonçalves, *ACS Appl. Mater. Interfaces*, 2020, **12**, 21020–21035.

41 E. Luong-Van, T. T. Madanagopal and V. Rosa, *Mater. Today Chem.*, 2020, **16**, 100250.

42 C. Tu, A. Bajwa, A. Shi, G. Wu and J. Wang, *Clin. Oral Investig.*, 2022, **26**, 2491–2502.

43 B. Kim, S.-H. Lee, S.-J. Song, W. H. Kim, E.-S. Song, J.-C. Lee, S.-J. Lee, D.-W. Han and J.-H. Lee, *Antioxidants*, 2019, **8**, 306.

44 Z. Liu, C. Yan, C. Kang, B. Zhang and Y. Li, *PLoS One*, 2015, **10**, e0116194.

45 W. Yao, T. Hadi, Y. Jiang, J. Lotz, T. J. Wronski and N. E. Lane, *Osteoporosis Int.*, 2005, **16**, 1939–1947.

46 N. E. Lane, J. M. Thompson, D. Haupt, D. B. Kimmel, G. Modin and J. H. Kinney, *J. Bone Miner. Res.*, 1998, **13**, 229–236.

47 W. Wang, J. R. P. Junior, P. R. L. Nalesso, D. Musson, J. Cornish, F. Mendonça, G. F. Caetano and P. Bártolo, *Mater. Sci. Eng., C*, 2019, **100**, 759–770.

48 B. F. Boyce and L. Xing, *Arch. Biochem. Biophys.*, 2008, **473**, 139–146.

49 C. Wang, H. Hu, Z. Li, Y. Shen, Y. Xu, G. Zhang, X. Zeng, J. Deng, S. Zhao and T. Ren, *ACS Appl. Mater. Interfaces*, 2019, **11**, 39470–39483.

50 A. Mazinani, M. J. Nine, R. Chiesa, G. Candiani, P. Tarsini, T. T. Tung and D. Losic, *Mater. Des.*, 2021, **200**, 109443.

51 Y. Luo, H. Shen, Y. Fang, Y. Cao, J. Huang, M. Zhang, J. Dai, X. Shi and Z. Zhang, *ACS Appl. Mater. Interfaces*, 2015, **7**, 6331–6339.

52 V. Rosa, H. Xie, N. Dubey, T. T. Madanagopal, S. S. Rajan, J. L. P. Morin, I. Islam and A. H. C. Neto, *Dent. Mater.*, 2016, **32**, 1019–1025.

53 P. Raz, T. Brosh, G. Ronen and H. Tal, *BioMed Res. Int.*, 2019, **2019**, 5163603.

54 M. Radenković, S. Alkildani, I. Stoewe, J. Bielenstein, B. Sundag, O. Bellmann, O. Jung, S. Najman, S. Stojanović and M. Barbeck, *Membranes*, 2021, **11**, 712.

55 A. Vajgel, N. Mardas, B. C. Farias, A. Petrie, R. Cimões and N. Donos, *Clin. Oral Implants Res.*, 2014, **25**, 879–893.

56 E. Chatzinikolaou and K. Keklikoglou, *Biodivers. Data J.*, 2021, **9**, e71542.